On-Demand Degradation of Metal–Organic Framework Based on Photocleavable Dianthracene-Based Ligand

Collet, Guillaume; Lathion, Timothee; Besnard, Céline; Piguet, Claude; Petoud, Stéphane

How to cite

COLLET, Guillaume et al. On-Demand Degradation of Metal–Organic Framework Based on Photocleavable Dianthracene-Based Ligand. In: Journal of the American Chemical Society, 2018, vol. 140, n° 34, p. 10820–10828. doi: 10.1021/jacs.8b05047

This publication URL: https://archive-ouverte.unige.ch/unige:108077
Publication DOI: 10.1021/jacs.8b05047

Publication: Collet, G.; Lathion, T.; Besnard, C.; Piguet, C.; Petoud, S., *J. Am. Chem. Soc.* **2018**, *140*, 10820-10828.

On-Demand Degradation of Metal-Organic Framework based on Photocleavable Dianthracene-based Ligand

Guillaume Collet,*,† Timothée Lathion,† Céline Besnard,‡ Claude Piguet,† Stéphane Petoud*,†,§

† Department of Inorganic and Analytical Chemistry, University of Geneva, 30 Quai E Ansermet, CH-1211 Geneva 4, Switzerland

‡ Laboratory of Crystallography, University of Geneva, 30 Quai E Ansermet, CH-1211 Geneva 4, Switzerland

§ Centre de Biophysique Moléculaire (CBM) ; UPR CNRS 4301, Rue Charles Sadron, F-45071 Orléans 2, France

KEYWORDS. Metal-organic framework, photocleavable ligand, trigger, controlled degradation, responsive material

ABSTRACT: We have designed a rigid photocleavable dianthracene-based ligand that reacts with ytterbium as coordination metal ion for the creation of a class of tridimensional light-degradable metal-organic framework (MOF). We demonstrated that we can obtain a high level of control on the disassembly of the MOF formed with this ligand which can be triggered either through light irradiation or temperature increase. The reversible 4π-4π photodimerization is the intrinsic chemical mechanism ruling the ligand and MOF cleavage. In the fields of biology and medicine, MOFs have sparked a strong interest as highly porous vehicles for drug release but have only been explored so far through the passive leakage of their payloads. The designed light-degradable MOFs can potentially overcome this limitation and serve as prototypes for drug delivery and corresponding therapeutic applications.

INTRODUCTION

Facing side effects related to detrimental interactions of active drugs (i.e. anti-inflammatory, chemotherapies) with healthy tissues or organs, an active research is performed to design vehicles able to safely carry the therapeutic compounds inside the body. Properly addressed at the place to cure by targeting or EPR effect (enhanced permeability and retention), such materials aim to restrict the delivery of drugs exclusively to the pathological tissue/organ. In such context, the loading capacity plays a central role for the efficiency of the delivery.

Initially described for gas storage, separation, catalysis, and sensing[2-5], Metal-Organic Frameworks (MOFs) are crystalline materials that were recently introduced in the field of biology and medicine for their high porosity offering unprecedented loading capacity of therapeutic payloads[6,7]. As an example, an impressive demonstration has been reported by Horcajada *et. al.* with the MIL-101 containing up to 1,376 grams of ibuprofen per gram of dehydrated MOF[9]. Several types of such materials are biocompatible and can be miniaturized to reach a nanometer range size compatible with applications in living organisms[10-13]. Obtained by the self-assembly between organic ligands and metals, MOFs can be produced in large amount and are easily purified and characterized due to their crystalline nature.

Despite all these advantages as carriers, they have so far only a limited development in therapeutic applications. Indeed, MOF have so far mainly been reported as "passive sponges" releasing their payloads out of the pores by slow diffusion[14,15]. New classes of responsive MOF that undergo changes resulting from external stimulation have emerged recently[16-18]. Couples of works report strategies to entrap the payload inside the MOFs pores such as using hydrophobic molecules or taking advantage of specific interactions within the cavities of the MOF without providing an effective control over the time and location of the releases of payloads[19]. We envisage as the major next breakthrough for the use of MOF in the fields of biology and/or medicine a specific mechanism to control the delivery of payloads at the right place and at the right moment.

The controlled disassembly of materials has been extensively studied since last decades to fulfil this demand. It has been successfully applied to polymeric nanoparticles[20-22], micelles[23,24], liposomes[25,26] or hydrogels[27-29] among others[30], reporting such smart materials as carriers for drugs delivery or as activatable probes for imaging[31,32]. These studies report interesting mechanisms with materials designed to specifically respond to endogenous triggers such as acidosis or oxidative stress linked to inflammation and tumors, but also to external triggers such as light irradiation[22,30,33]. External triggers such as light have the advantage of

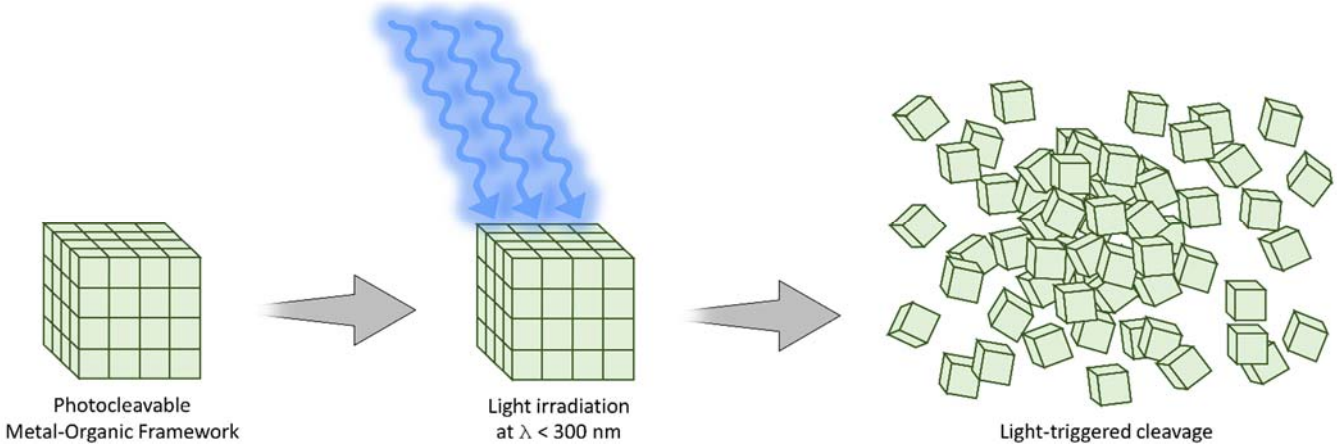

Figure 1. Overview of the light degradable MOF behavior upon light irradiation. In this schematic representation, the CD-MOF-161 which is a photocleavable metal-organic framework, is exposed to a UV light beam (wavelength below 300 nm). The light reaching CD-MOF-161 crystal induces the cleavage of the ligands located within the crystal structure which falls apart.

providing an "on-demand" release with a high level of control over time and location[30]. Moreover, the degradability of such materials is a great advantage for their administration in living organisms since particles will fall apart as small size fragments that can be cleared out of the body (i.e. urine), thus avoiding or reducing their massive accumulation in filtering organs such as the liver[34,35].

In this report, we bridge the gap between light-degradable materials and Metal-Organic Frameworks by synthesizing a MOF that is made photocleavable on-demand due to the light-responsive nature of its organic ligand. This ligand photocleave upon light exposure at a specific wavelength (<300 nm) or a raise of the temperature, as illustrated in Figure 1. If some works describe photoactive behaviors of MOFs such as the already described UiO-AZB[36], MIL-100[37], UiO-66[38,39] or with the Ph-An-COF presenting a photoinduced structural change[40], to the best of our knowledge, no such system has been reported so far. The challenge was to achieve such control with a ligand possessing the rigidity required for the formation of MOFs. Among molecular mechanisms reported for controlled degradation, the anthracene and its derivatives are interesting since they undergo a light-driven reversible 4π-4π photodimerization leading to the formation of rigid photodimers upon light irradiation above 350 nm whereas wavelengths below 300 nm induce their photocleavage.

To establish a proof-of-principle, the 9-anthracene carboxylic acid (9AC) was photodimerized by irradiation at 365 nm to yield the 9-anthracene carboxylic acid dimer (Di-9AC). Its light-induced cleavage was extensively tested using two irradiation sources: a continuous UV lamp at 254 nm and a pulsed laser at 266 nm. The temperature-induced cleavage of anthracene dimers was also tested with Di-9AC. After full characterization and validation of its ability to be cleaved in a triggered way, the synthesized Di-9AC was used as ligand for MOFs synthesis. As a result, a novel tridimensional crystalline network was formed with the two carboxylic groups of the Di-9AC ligands, bridging a dinuclear clusters of ytterbium used as coordination metal ions. This 3D lanthanoid metal-organic frameworks (Ln-MOF) was named CD-MOF-161, for Controlled Degradable Metal-Organic Framework, and its structure was characterized by single-crystal X-ray diffraction. To investigate the controlled disassembly of CD-MOF-161, the same light sources mentioned for the Di-9AC ligand studies (254 and 266 nm) and a raise of the temperature (160°C) were used as triggers for the degradation. In both cases, the triggers led to the photocleavage of the Di-9AC in CD-MOF-161 structure that fell apart.

RESULTS AND DISCUSSION

Synthesis and characterization of the Di-9AC ligand. Anthracenes and their derivatives are known to undergo a [4+4] photodimerization upon light irradiation (λ > 350 nm) to yield the corresponding anthracene dimers[4,41,42]. Due to the C_s-symmetry point group adopted by the 9-anthracene carboxylic acid (9AC), two geometrical isomers of the dimeric 9-anthracene carboxylic acid (Di-9AC) could be formed: the head-to-head (*hh)* dimer, and the head-to-tail (*ht)* dimer resulting from the stacked (*hh*) or opposite (*ht*) arrangements of the carboxylic groups. According to previous studies[42], the formation of the *hh* dimer in solution is prevented by the steric hindrance occurring

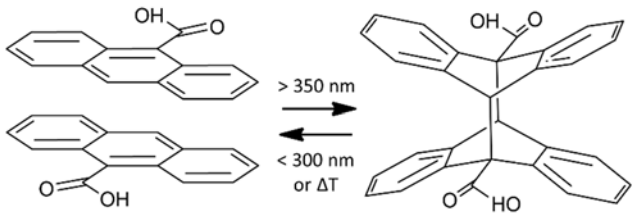

Scheme 1. Scheme of the reversible photodimerization mechanism. Overview showing the photodimerization of the 9AC into Di-9AC under a wavelength superior to 350 nm UV light exposure and the photocleavage when exposed either to UV light below 300 nm or to a raise of the temperature.

between the two carboxylic acid side chains and, as a result, only the *ht* dimer is obtained (Scheme 1). The ^{1}H NMR chemical shift of the bridgehead proton allows for an unambiguous differentiation in solution between the two isomers due to distinct chemical environments. Based on works published by Ito *et. al.,* the chemical shift (DMSO-d_6) of the bridgehead proton in the *ht* dimer is δ = 5.63 ppm[41]. These results match with our own as we observe a chemical shift for the bridgehead proton at 5.62 ppm in DMSO-d_6 (Figure S1), indicating the exclusive formation of the desired *ht* Di-9AC dimer in solution. This *ht* dimer is preferred since diametrically opposed carboxylic acid groups constitute an favorable shape for the formation of MOFs. The formation of the dimeric 9-anthracene carboxylic acid (Di-9AC) in the desired *ht* orientation was confirmed by X-ray diffraction on collected crystals (Table S1-3 and Figure S5-7) and by ^{1}H and ^{13}C NMR spectra in solution (Figure S1-4). The Di-9AC formation was also studied by UV-Vis and FTIR absorbance spectroscopies. The comparison of the FTIR spectra for 9AC (Figure S9) and Di-9AC (Figure S8) reveals the typical signals reported by More *et. al.* with an intense vibration at 1682 cm^{-1} assigned to the typical CO stretching of 9AC and with a series of broad vibrational signals in the 2800 to 3650 cm^{-1} range assigned to CH and OH stretching vibrations. The formation of the Di-9AC is revealed by the disappearance of the signal at 1682 cm^{-1} corresponding to the CO stretching vibration observed on the 9AC monomer[43] (Figure S8-9). Moreover, the presence of two well-defined vibrations at 1450 and 1470 cm^{-1} (splitting of C–O bonding) is a good indication of the presence of an anthracene photodimer[44]. The UV-Vis absorption spectrum of the Di-9AC does not show the characteristic absorption bands between 300 and 400 nm, which can be observed for the 9AC (Figure S10). This observation is due to the photodimerization process that disrupts the conjugation of anthracene, generating four o-xylene chromophores[44]. Similarly, in the solid-state diffuse reflectance spectrum, no signal can be detected from 300 to 400 nm for the Di-9AC (Figure S11) indicating that the behaviors are the same in presence and in absence of solvents.

Di-9AC cleavage upon light exposure or raise of the temperature. The cleavability of the synthesized Di-9AC was first validated by thermocleavage experiments. ^{1}H NMR experiments showed that the incubation of the Di-9AC dimer at 130°C leads to its gradual degradation over

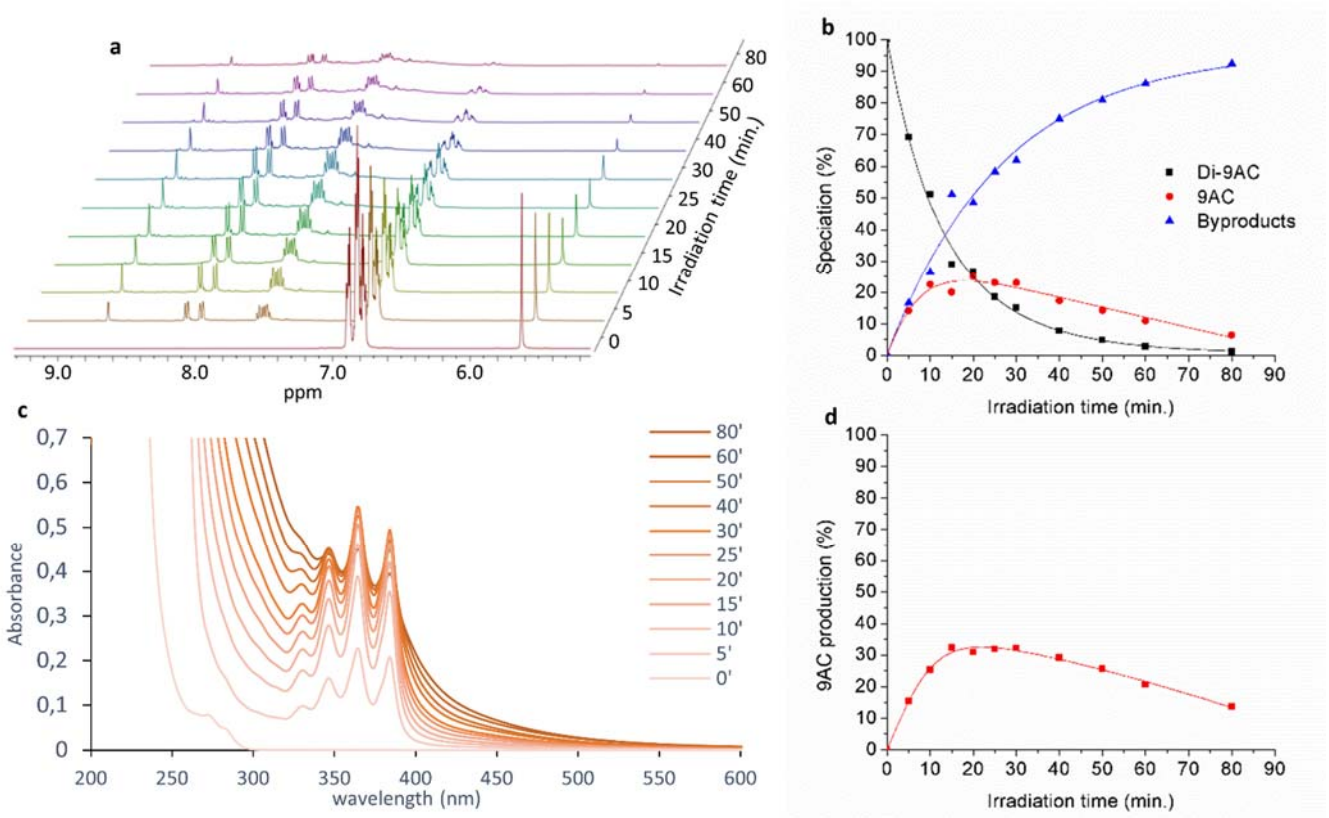

Figure 2. Controlled degradability of the Di-9AC ligand. (a) ^{1}H NMR spectra of the Di-9AC collected after increasing irradiation times with a pulsed laser at 266 nm wavelength. (b) Quantification by ^{1}H NMR of the photocleavage of the Di-9AC into 9AC and byproducts obtained at different irradiation times at 266 nm. (c) UV-Vis absorbance spectra showing the appearance over time of the 9AC upon the irradiation of the Di-9AC at 266 nm. (d) Quantification by UV-Vis absorbance of the 9AC at different irradiation times at 266 nm.

time into the 9AC monomer (Figure S12). This degradation profile was confirmed by UV-Vis absorbance spectroscopy experiments, quantifying the appearance of the characteristic bands of 9AC between 300 and 400 nm as shown in Figure S13. The photocleavability of the Di-9AC was demonstrated with two different irradiation sources, respectively a 266 nm pulsed laser and a continuous 254 nm UV-Pen (spectra provided in Figure S14). The Di-9AC presents a high energy $\pi \rightarrow \pi^*$ absorption at these two wavelengths that allows its photocleavage[45]. In both cases, this process was followed by ^{1}H NMR (Figure 2a and Figure S15a) to determine the speciation curves presented in the Figure 2b (Figure S15b). The irradiation-driven cleavage of the Di-9AC is clearly demonstrated with the concomitant appearance of the 9AC and some byproducts. The photocleavage was also followed by UV-Vis absorbance spectroscopy (Figure 2c-d and Figure S15c-d) showing the gradual appearance of the typical bands of the 9AC with increasing irradiation time. The quantification of the 9AC on the basis of UV-Vis spectra is perfectly correlated with the NMR data (Figure 2b, d and Figure S15b, d). A faster degradation kinetic was observed upon laser irradiation compared to UV-Pen in direct correlation with the irradiation power. Since the temperature is known to rule the cleavage of the dimeric anthracene[45], similar studies by ^{1}H NMR and by UV-Vis absorbance spectroscopy were realized upon heating at 130°C (Figure S16). As an advantage of the temperature-induced cleavage of the Di-9AC over the light-irradiation, any byproducts were observed (Figure 2 and Figure S15 and S16).

Synthesis of the Di-9AC-based metal-organic framework and analysis of its structure. Having confirmed the formation of the pure *ht* Di-9AC isomer and its controlled degradability, a MOF was successfully assembled with the ytterbium (Yb^{3+}) as coordination metal ion to give a material with the formula $[Yb_2(Di\text{-}9AC)_2(DMA)_2(acetate)_{0.76}(formate)_{1.24}]$ (Figure 3b). This novel MOF assembled from this Di-9AC ligand was named CD-MOF-161 (Controlled Degradable Metal-Organic Framework). CD-MOF-161 crystallizes in the triclinic space group $P\bar{1}$. The asymmetric unit is shown in Figure S17. Interestingly, the CD-MOF-161 contains Yb dinuclear clusters as secondary building units, as shown in Figure 3a. The two Yb^{3+} ions of the cluster are bridged by one acetate and one carboxylate group belonging to one Di-9AC ligand. A second acetate shares one oxygen atom located between the two ytterbium atoms while his second oxygen atom is only bound to one of the ytterbium atom (Yb1). Yb2 is therefore coordinated to one Di-9AC (O11, O12), one bridging Di-9AC (O10), one DMA molecule (O14), one bridging acetate (O9), one shared acetate (O8, O15) and a water molecule (O13). On its side, Yb1 is coordinated to two Di-9AC (O1 O2 and O3 O4), the bridging Di-9AC (O6) the bridging acetate (O5), the shared acetate (O15) and one DMA molecule (O7). This analysis reveals a total coordination number of 8 for both Yb1 and Yb2 with an Yb-Yb distance of 4.2584(5) Å. The Yb-O distances span from 2.242(3) to 2.451(6) Å (Table S5). Crystal data for CD-MOF-161 are summarized in Table S4.

The SHAPE software[46] was used to analyze the shape of the coordination polyhedron around lanthanide cations by calculating continuous shape measures (CShM) between the observed coordination polyhedrons and idealized ones. The shape is closely related to several ideal polyhedrons

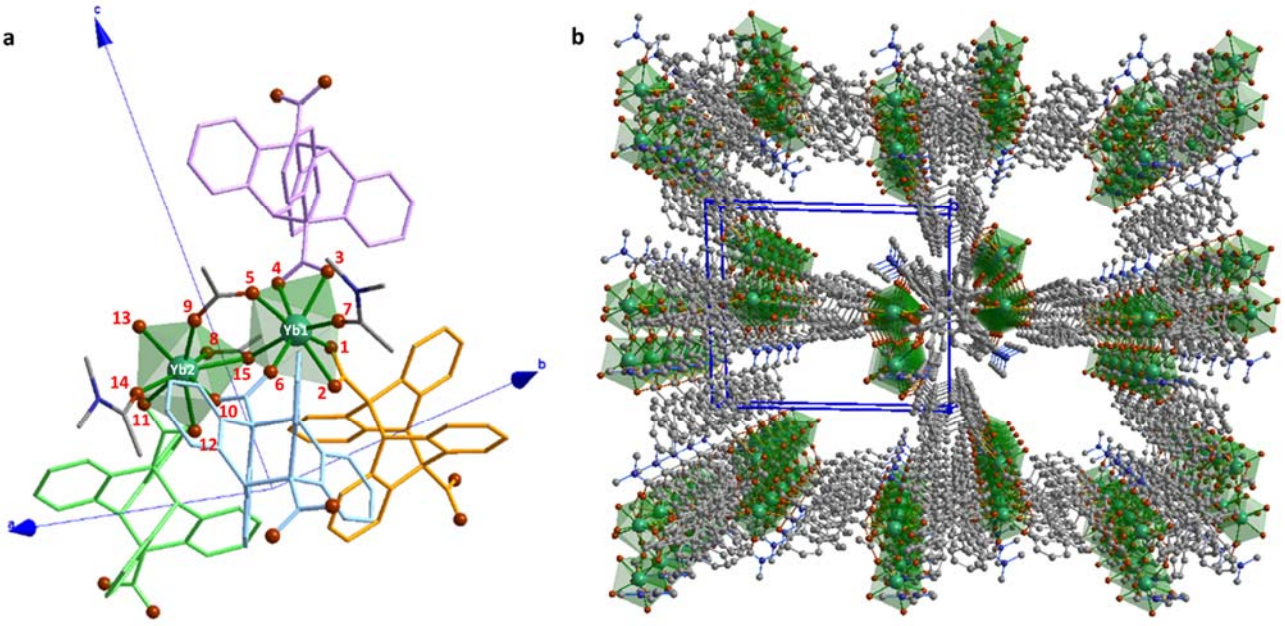

Figure 3. Structure of the controlled degradable MOF. Pictures of the crystal structure of (a) the asymmetric unit of CD-MOF-161, (b) the 3D framework of CD-MOF-161 with cell (blue). (a, b) Hydrogen atoms are omitted for clarity.

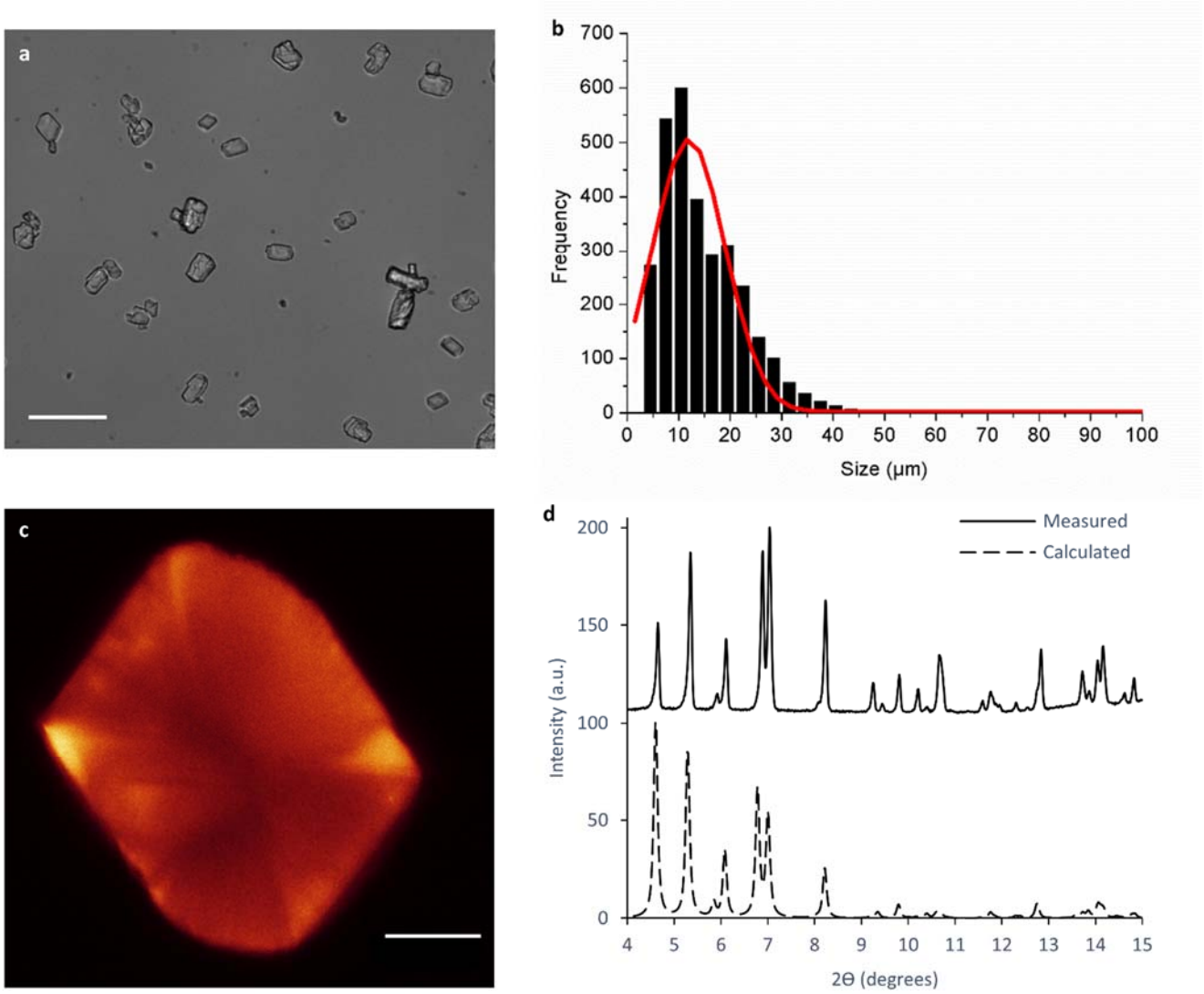

Figure 4. Characterization of the controlled degradable MOF. (a) Bright field microscopy image of the as-synthesized CD-MOF-161. Scale bar is 100 µm. (b) CD-MOF-161 size distribution histogram (black) obtained from bright field images analysis and gaussian fitting (red). (c) 0.803 µm thickness optical section of a fluorescein-loaded CD-MOF-161 obtained by confocal fluorescence microscopy. Scale bar is 10 µm (d) Experimental (continuous line) and calculated (dashed line) powder diffraction patterns. The calculated pattern was calculated with mercury[1] software using the single-crystal structure recorded at 180K and correcting the unit-cell parameters for the temperature difference. The room-temperature unit-cell parameters were obtained doing a Le Bail profile fitting in the TOPAS software[8] of the experimental diagram and are a=16.84 Å, b=18.33 Å, c=19.52 Å, α=85.671°, β=79.06°, γ=65.63°.

(see table Figure S18) but one can conclude that the Yb atom is in a distorted dodecahedral environment. The two polyhedrons share a corner to form the dinuclear cluster, with an Yb-Yb distance of 4.2584(5) Å. The Yb-O distances span from 2.242(3) to 2.451(6) Å (Table S5).

Experimental data showing the coordination of Yb^{3+} ions with the Di-9AC ligand were obtained by comparing results of FTIR absorption spectra of the free Di-9AC and of the MOF formed with this dimer (Figure S19). The carboxylic groups are the main groups in the structure of Di-9AC which undergo a transformation during the deprotonation and metal complexes formation. The broad band at 3032 cm^{-1} assigned to the ν(OH) stretching vibrations of the carboxylic acid groups and the bands around 1700 cm^{-1} assigned to the stretching vibrations ν(C=O) of carboxylic groups of the Di-9AC disappear in the spectrum collected on the MOF due to the complete deprotonation of carboxylic groups and coordination with Yb metal ions. Strong bands assigned to the asymmetric $\nu_{as}(COO^-)$ and symmetric $\nu_{s}(COO^-)$ stretching vibrations of carboxylate anion appear in the MOF around 1406 cm^{-1} and around 1558-1597

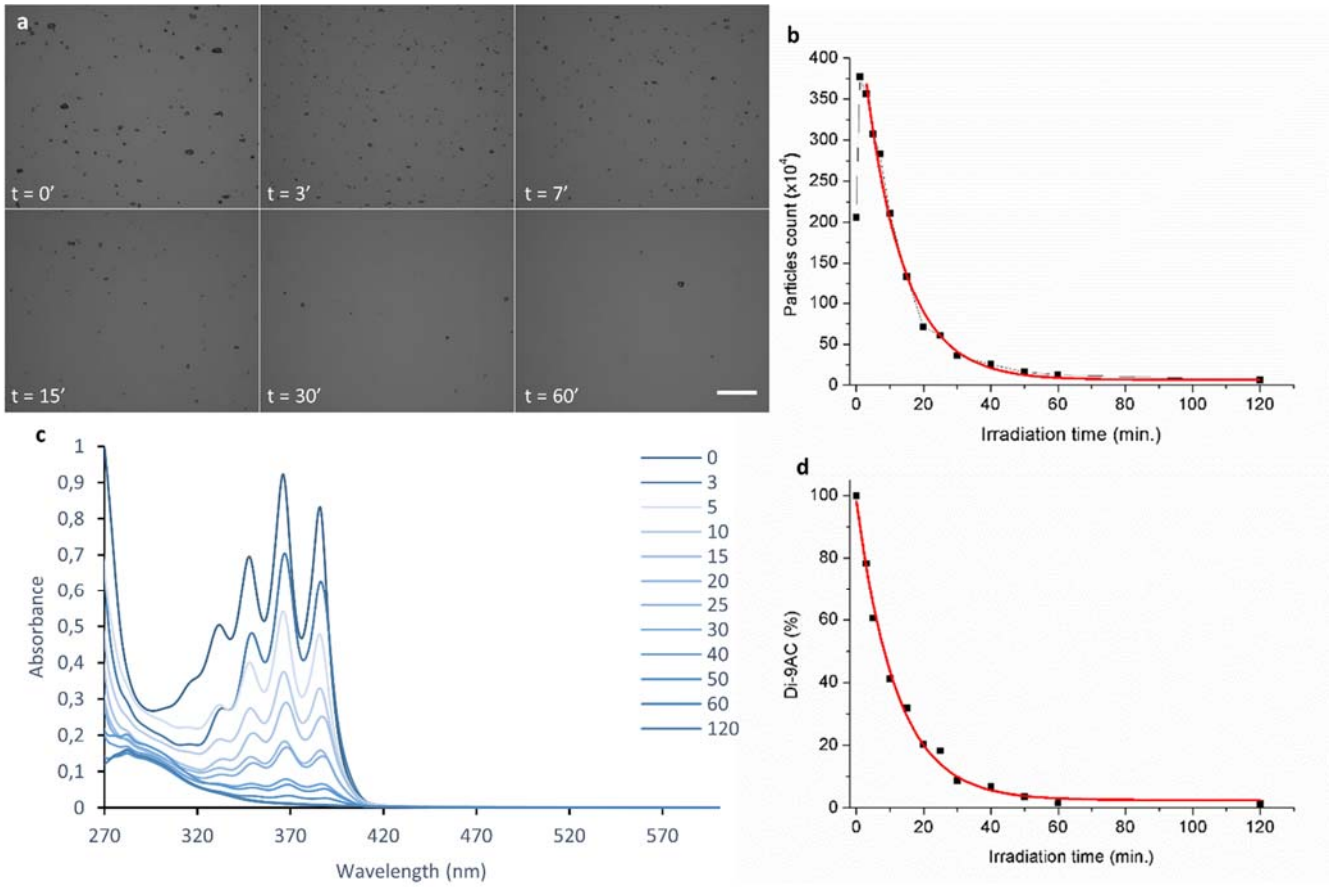

Figure 5. Controlled degradation of the light degradable MOF. (a) Bright field microscopy images of a CD-MOF-161 suspension irradiated during various times with a pulsed laser at 266 nm wavelength. Scale bar is 200 µm (b) Quantification of the number of CD-MOF-161 particles along the irradiation time with a 266 nm pulsed laser obtained from the analysis of bright fields microcopy images (black) and exponential decay fitting (red). (c) UV-Vis absorbance spectra of 9AC resulting from the thermocleavage of left CD-MOF-161 collected after various times of irradiation with a pulsed laser at 266 nm wavelength. (d) Quantification by UV-Vis absorbance spectroscopy of the ligand of the left CD-MOF-161 after the irradiation times with a 266 nm pulsed laser (black) and exponential decay fitting (red).

cm^{-1}. These data reveal changes of the Di-9AC ligands in the MOF when coordinated with Yb^{3+} cations[47].

The dinuclear clusters are interconnected together to form a 3D network. A topological analysis was carried out in order to gain a deeper level of understanding of the nature of this framework. Clusters forming four-connected vertexes are connected via the Di-9AC ligands forming two connected edges (Figure S20). This organization results in a diamond net with RCSR (Reticular Chemistry Structure Resource database) symbol dia[48]. The packing of the clusters in the MOF and the underlying net are depicted in Figure S21. The Di-9AC ligand maintains its original shape in the structure without any distortion or π–π stacking effect. From the perspectives of the crystallographic directions, three types of 1D microporous channels can be found in CD-MOF-161, as shown in Figure S22. These channels are interconnected. Using PLATON software[49], the potential solvent volume was estimated to fill about 47 percent of the unit-cell volume on the basis of a probe size of 1.2 Å and a grid of 0.2 Å.

Crystals collected after synthesis were studied by powder X-ray diffraction (PXRD) to compare the patterns obtained experimentally with the one computed from the single crystal structure. The theoretical peaks are clearly identified in the experimental sample as shown in Figure 4d and no additional diffraction peaks were found, indicating the synthesis of a unique crystalline entity. This result, in combination with results of elemental analysis fitting well with the molecular formula of the measured structure for CD-MOF-161, allows to conclude that our synthesis method leads to a unique and pure MOF.

Thermo-gravimetric analysis (TGA) of the dried MOF showed a first weight loss from 20 to 200°C which is attributed to the loss of a molecule of water, DMA and formate (2 molecules each) (-14% experimental weight loss, -18% calculated). A second weight loss from 200 to 550°C is attributed to the loss of the remaining organic content of

the MOF which correspond to the two Di-9AC ligands (-60% experimental weight loss, -58% calculated). Above 550 up to 1000 °C, no weight loss was observed, with an experimentally remaining weight of 26%, corresponding to the inorganic content of the MOF (i. e two Yb(III) as Yb_2O_3, calculated remaining weight: 26%) (Figure S23).

Brightfield optical microscopy analysis was used to evaluate the size distribution of CD-MOF-161. Quantifications on experimental pictures show an average size of 11.97 µm with a polydispersity of 58.84% (Figure 4a and 4b).

In order to visualize the microscopic structure of crystals, an optical sectioning was obtained by confocal microscopy of a CD-MOF-161 incorporating fluorescein. A picture is presented on the Figure 4c for a 0.803 µm thickness section. To do so, fluorescein molecules were incorporated in the MOF during the synthesis. This confocal imaging method allows to observe only a thin section of the crystal without the contributions of the plans located above and below the imaging plan. Such observation of the MOF through the fluorescence of the fluorescein it contains reveals the shape of the crystal in the plan of the imaging. This result indicates that the fluorescent dye is located in the core of the MOF therefore demonstrating that its pores can loaded with such molecules. No change of the crystalline structure is observed when pores contain fluorescein molecules (Figure S28).

The potential toxicity of the CD-MOF-161 particles and the $Yb(OAc)_3$ was assessed by a series of cytotoxicity experiments on a model of cell line (HeLa cells). Results show that the presence of ytterbium acetate up to 1 mM does not induce any significant cell toxicity after 24h and 48h of incubation. A toxicity associated with CD-MOF-161 was observed when a large number of MOFs where present with cells. Interestingly, the MOF that have been washed with water appear to be less toxic. It could be associated with the release of DMA (synthesis solvent) from the pores through this washing process (Figure S29-31).

Controlled disassembly of the MOF upon light irradiation or temperature. The ability of CD-MOF-161 to degrade upon trigger addition, either light irradiation or raise of temperature was determined through a microscopy-based experiment, quantifying the number of microparticles present per field of view over time (Figure 5a and Figure S24a and S25a). A suspension of CD-MOF-161 in DMA was exposed to a 266 nm pulsed laser irradiation. Microscopy-based quantifications reveal that the number of CD-MOF-161 particles exponentially decreases along the irradiation time as presented in the Figure 5b. Similar observations could be obtained upon exposition to UV-Pen irradiation except that a longer time is required to get all particles photocleaved due to the lower power of the irradiation source (Figure S24a). Interestingly, an increase by a factor 2 of the counted particles was observed after few minutes of irradiation resulting from the individualization of some aggregated CD-MOF-161 crystallites present after the synthesis.

Compared to light-induced degradation, the raise of temperature up to 160°C induces the thermocleavage of the ligand and the resulting MOF disassembly with the same decreasing exponential profile. However, before its exponential decrease, an increase of a factor 15 of the initial number of particles is observed (Figure S25a). This important increase can be due to the mechanism of degradation involved and the type of employed trigger (either light irradiation or raise in temperature). The light-induced cleavage of CD-MOF-161 results mainly from an erosion process by exposing the surface of crystals to light irradiation whereas the temperature is transmitted to the entire CD-MOF-161 crystals and is not restricted to their surfaces. The thermocleavage of ligand inside the CD-MOF-161 structure compromises its structural integrity, resulting in fragmentation processes of crystals.

Molecular evidences for the controlled degradation were obtained through the quantification by UV-Vis absorbance spectroscopy of the Di-9AC ligand from left undegraded CD-MOF-161 (see methodology in Figure S27). To do so, at each time point of the kinetic experiment, the left CD-MOF-161 were collected and thermocleaved at 160°C for 48h, resulting in i) the complete disassembly of CD-MOF-161 crystals, ii) the complete cleavage of Di-9AC ligands. The resulting 9AC and its typical bands were quantified and plotted as function of time to obtain the profile represented on Figure 5c, d (and Figure S24c, d and S25c, d). These data combined with results of the particles counting show that the CD-MOF-161 degrades upon trigger addition, either with light irradiation (<300 nm) or raise of temperature.

CONCLUSION

By designing a photocleavable dianthracene-based ligand, we created a system for which we obtained a high level of control for the disassembly of the corresponding MOF which can be triggered either through light irradiation or temperature increase. The Di-9AC ligand has been extensively characterized using different experimental techniques. We have demonstrated that the cavity of this MOF can be used to incorporate molecules such as fluorescein.

We successfully established in this work the first proof-of-principle of a light-degradable metal-organic framework that is obtained photocleavable by design and operating on-demand. The use of light presents the advantage to be an external stimulus that acts in a remote-control manner, turning ON and OFF the degradation on-demand at desired times and locations[29]. Future developments of this MOF family will open exciting perspectives toward advanced medicine, in particular, would allow researchers to remotely induce release of molecules in living organisms, or, eventually, physicians to spatiotemporally control drugs release in patients.

EXPERIMENTAL SECTION

Materials. Anthracene-9-carboxylic acid (9AC, 99%, Acros Organics), tetrahydrofuran (THF, Fisher Scientific), deuterated dimethyl sulfoxide (DMSO-d6, D, 99.9%, Cambridge Isotope Laboratories Inc.), ytterbium(III) acetate

hydrate (Yb(OAc)3, Aldrich), ammonium formate (Fluka), ammonia solution (25%, VWR chemicals), Fluorescein sodium salt (Fluka), N,N-dimethylacetamide (DMA, 99+%, Acros Organics), acetonitrile (99.95%, VWR chemicals) were used as received.

General Procedures and Instrumentation. ^{1}H and ^{13}C NMR spectra were recorded at room temperature on a Bruker Avance 400 MHz spectrometer. Chemical shifts are given in ppm with respect to TMS. Pneumatically-assisted electrospray (ESI-MS) mass spectra were recorded on an Applied Biosystems API 150EX LC/MS system equipped with a Turbo Ionspray source®. Elemental analyses were performed by the Microchemical Laboratory of the University of Geneva (Unige) and the Supramolecular Chemistry Laboratory at the Ecole Polytechnique Fédérale de Lausanne (EPFL). Thermogravimetric analyses (TGA) were performed on a Mettler Toledo TGA/DSC 1 STARe System under a nitrogen flow. Several milligrams of sample were put in an aluminum oxide cell, and the cell was heated to 1000°C with a heating rate of 5°C/min. The mathematical analyses were performed using OriginPro8 (OriginLab) and Excel® (Microsoft) softwares.

Synthesis and Characterization of the Di-9AC. The head-to-tail 9-anthracene carboxylic acid dimer (Di-9AC) was prepared according to the procedure published by Nofen *et. al.*[42]. Briefly, 10.10 g of 9AC (45.45 mmol) were dissolved in 200 mL of degassed THF under nitrogen atmosphere and vigorous magnetic stirring. The reaction was maintained in darkness and the solution was photo-irradiated for four days using two UV bench lamps (λ = 365 nm, VL-6-LC, Vilber-Lourmat, 6 watts each, with a light density of approximately 610 µW/cm² located at a distance of 15 cm from the reaction, spectra in Figure S26). A white precipitate appeared which was collected by filtration using a Büchner funnel and washed repeatedly with cold THF (2 x 5 mL) and cold water (2 x 5 mL). The collected solid was then dried for 24 h under high vacuum to yield 5.59 g (12.59 mmol, η = 55 %) of Di-9AC as a white powder. ^{1}H NMR (DMSO-d_6, 400 MHz, 298 K) δ ppm: 13.60 (2H, bs), 6.90-6.85 (4H, m), 6.84-6.82 (8H, m), 6.78-6.74 (4H, m), 5.62 (2H, s).^{13}C NMR (DMSO-d_6, 100 MHz, 298 K) δ ppm: 174.40, 142.60, 141.90, 127.46, 126.53, 125.77, 125.36, 65.52, 54.40. ESI-MS (soft neg., $MeOH/H_2O/NEt_3$ 49.5/49.5/1.0, m/z): [di-9AC-H]$^-$: 443.25 (exp.), 443.13 (calc.); [(di-9AC)$_2$-H]$^-$: 887.55 (exp.), 887.27 (calc.). Elemental analysis calculated for $C_{30}H_{20}O_4$: C 81.07, H 4.54; found: C 81.23, H 4.46.

X-ray Crystallography of Di-9AC. A slow evaporation of concentrated DMA solutions (Table S3 and Figure S7) and DMSO solution (Table S1 and Figure S5) of Di-9AC led to the formation of X-ray quality prisms suitable for single crystal analysis and structure determination. Other crystals of Di-9AC were obtained in DMA by warming up the solution to 130°C and then by cooling down to room temperature (Table S2 and Figure 5).

Optical Spectroscopy. Diffuse reflectance spectra were collected on solid samples on a Perkin Elmer Lambda 900 equipped with a 60 mm Labsphere integration sphere specifically designed for this instrument. Absorbance spectra were recorded in solution (in H2O with 0.5% of NH3) with a Perkin-Elmer Lambda 1050 spectrometer using quartz suprasil cells of 1 cm optical path length. For quantifications (Figure 2d and Figure S15d, S16d), a post-acquisition signal processing was applied to subtract the contribution of the UV-absorbing byproducts generated during light irradiations. FT-IR spectra were measured using a Bruker Tensor 27 spectrometer.

Synthesis of CD-MOF-161. The reaction of ytterbium acetate and Di-9AC was prepared in a 4:1 (metal:ligand) ratio in 2.3 mL of DMA by mixing 68 µmol of $Yb(OAc).H_2O$ (23.81 mg) with 17 µmol of Di-9AC (7.56 mg). The mixture was sealed in a Pyrex tube, heated at 60°C for 2 days, and then cooled to room temperature at a rate of 2°C/hour. The resulting colorless block crystals were obtained and washed with DMA to remove the unreacted materials. Larger crystals were obtained by the addition of 138 µmol of ammonium formate (8.70 mg) into the mixture prior heating[50,51]. Fluorescein-loaded crystals of CD-MOF-161 were obtained by the addition of 5 µmol of fluorescein sodium salt (1.88 mg) into the mixture prior heating. To perform the elemental analysis, the as-synthesized CD-MOF-161 crystals were extensively washed with DMA and then with acetonitrile to be further dried for 48 h under high vacuum (8.10^{-6} mbar) to yield between 12.5 and 12.9 mg of MOF. η = 96-99 % (based on Di-9AC). Elemental analysis calculated for $C_{71}H_{60}N_2O_{15}Yb_2$: C, 55.83; H, 3.96; N, 1.83. Found: C, 56.04; H, 4.14; N, 1.81.

X-ray Structure Determination for $[Yb_2(C_{30}H_{18}O)_2(C_4H_9NO)_2(C_2H_3O_2)_{0.76}(CHO_2)_{1.24}]$. A single-crystal of CD-MOF-161 was deposited into a Mitegen cryoloop in fomblin oil. Data were collected at 180K on an Agilent Supernova diffractometer equipped with an Atlas CCD detector. Details of the crystallographic refinement, carried out in SHELXL[52] using Olex2[53], can be found in Supplementary Table 4. Two disordered DMA molecules are coordinated to the metals. They were refined using two components. Geometrical restraints (SADI for the Yb-O distances) were applied, as well as restraints (RIGU)/constraints (EADP on close atoms) on anisotropic displacement parameters. Acetate/formate molecules are present in the coordination sphere of the Yb atoms. A mixed acetate/formate model was therefore used. DFIX was applied on the C-C acetate distance for one (C52-C53) acetate. Restraints were applied on anisotropic displacement parameters (RIGU). An oxygen atom is observed that can be either attributed to a water molecule present in the coordination sphere of Yb^{3+} or to a highly disordered DMA molecule for which only the position of the oxygen atom is well-defined. No satisfactory model could be found so that the water molecule was chosen. Disordered solvent molecules present in the channels of the MOF were taken into account by using the squeeze/bypass method[54] as implemented in Olex2 software. Before this squeeze/bypass procedure, the R factors were R1 = 0.1090, wR2 = 0.2898. A void of about 2500 Å^3 was found as a cavity of the MOF

containing about 885 electrons. This value corresponds to the presence of about 18 molecules of DMA par unit-cell (9 per formula unit). The "squeezed" molecules were not added to the formula unit so that the density and the absorption coefficient are somehow lower than expected. A view of the asymmetric-unit depicted at 50 percent probability is shown in Figure S17.

Light Irradiation for Photo-degradation. A Quantel® Nd-YAG Q-smart 850 laser that is pulsed at 10 Hz was used to obtain photons a 266 nm (selection of the fourth harmonic of the fundamental 1064 nm). The beam of this laser at 266 nm is around 7 mm in diameter with a measured power of 1.30 W. As continuous light source, a short-wave UV quartz pencil lamp (Pen-Ray® mercury light source, Edmunds Optics) was used, emitting a light at 253.7 nm with an output power density of approximately 4.5 mW/cm2.

MOF Sizing and Counting. The as-synthesized CD-MOF-161 size distribution was determined by microscopy-based method using a Tali™ Image-Based Cytometer (Invitrogen™). 25 uL of the MOF suspension was introduced in the measurement chamber of an analysis slide. The Tali™ was set to acquired 20 fields of view per sample. The analysis of the 20 acquired pictures were performed by ImageJ software using the 'analyze particles' plugin on previously binarized and thresholded pictures. The size distribution was fitted by a Gaussian curve with OriginPro8 software. The mean particle size and the polydispersity were determined from this fit. Polydispersity (%) = standard deviation / average particles size x 100. For degradation analysis of CD-MOF-161 over time upon trigger addition (light or temperature), the same analysis was performed, extracting the total count of particles per time point.

MOF Optical Imaging. Optical microscopy was realized at the Bioimaging Center of the University of Geneva, Switzerland. Brightfield microscopy images of MOF crystals was acquired with an Axio Imager Z1m from Zeiss equipped with a high resolution sCMOS Hamamatsu camera Flash4.0. Confocal fluorescence imaging of fluorescein-loaded MOF crystals was performed with an inverted confocal microscope Leica SP8. The fluorescein dye located inside of the MOF pores was excited with a 488 nm laser while the emitted fluorescence was selectively collected with the HyD Leica detector from 515 to 545 nm. The pinhole was set to obtain optical sections of 0.803 µm thicknesses.

Cell Cytotoxicity. HeLa cells (ATCC) were cultured in EMEM medium (ATCC) supplemented with 10 % (vol:vol) Fetal Bovine Serum (FBS, Sigma), 100 U/ml penicillin (Sigma), 100 µg/ml streptomycin (Sigma). Cells were routinely cultured at 37 °C in a humidified incubator in a 95 % air/5 % CO2 atmosphere and passaged by detaching cells with 0.05 % trypsin-EDTA solution (Gibco). HeLa cells were seeded in a 96 well plate at 5000 cells/well in a final volume of 200 µL of complete medium. After 24h, cell culture medium was removed and compounds to be tested were added at various concentration, either CD-MOF-161 or $Yb(OAc)_3$. The toxicity of these compounds was evaluated after 24h and 48h of incubation by the Alamar Blue™ Cell Viability Reagent (Invitrogen). Briefly, compounds were removed and cells were washed once with PBS (with Ca^{2+}/Mg^{2+}) before the incubation at 37 °C with the Alamar Blue™ reagent diluted to 1:10 in PBS, final volume of 200 µL/well. After 2-3h at 37 °C, the fluorescence of the 96 well plates were read with a Victor³™V plate reader (Perkin Elmer, excitation filter 560/10 nm, emission filter 605/10 nm). Cell viability was expressed in %, considering the untreated cells as the reference for 100% of viability.

ASSOCIATED CONTENT

Supporting Information.

The Supporting Information is available free of charge via the Internet at http://pubs.acs.org."

Additional supplementary figures about absorption spectroscopy measurements, ^1H and ^{13}C NMR spectroscopy, thermogravimetric analysis, crystallographic data and tables, FT-IR spectroscopy measurements, and particles counting.

AUTHOR INFORMATION

Corresponding Author

* guillaume.collet@cnrs-orleans.fr
* stephane.petoud@inserm.fr

Author Contributions

The manuscript was written through contributions of all authors. All authors have given approval to the final version of the manuscript.

Notes

The authors declare no competing financial interest.

ACKNOWLEDGMENT

The authors gratefully acknowledge the Swiss National Science Foundation for financial support (grant numbers 200020_159881 and 206021_164019) as well as la Ligue Nationale Contre le Cancer, la Région Centre, l'Agence Nationale de la Recherche (NIRA – ANR-13-BS08-0011). S.P. acknowledges support from the Institut National de la Santé et de la Recherche Médicale (INSERM). Authors are also grateful to Kerry-Lee Buchwalder and to Dr. Euro Solari for elemental analyses and to Jérôme Bosset for the microscopy.

REFERENCES

(1) Macrae, C. F.; Bruno, I. J.; Chisholm, J. A.; Edgington, P. R.; McCabe, P.; Pidcock, E.; Rodriguez-Monge, L.; Taylor, R.; van de Streek, J.; Wood, P. A. *J. Appl. Cryst.* **2008**, *41*, 466.

(2) Kreno, L. E.; Leong, K.; Farha, O. K.; Allendorf, M.; Van Duyne, R. P.; Hupp, J. T. *Chem. Rev.* **2012**, *112*, 1105.

(3) Furukawa, H.; Cordova, K. E.; O'Keeffe, M.; Yaghi, O. M. *Science* **2013**, *341*, 974.

(4) Li, J. R.; Kuppler, R. J.; Zhou, H. C. *Chem. Soc. Rev.* **2009**, *38*, 1477.

(5) Murray, L. J.; Dinca, M.; Long, J. R. *Chem. Soc. Rev.* **2009**, *38*, 1294.

(6) Horcajada, P.; Chalati, T.; Serre, C.; Gillet, B.; Sebrie, C.; Baati, T.; Eubank, J. F.; Heurtaux, D.; Clayette, P.; Kreuz, C.; Chang, J. S.; Hwang, Y. K.; Marsaud, V.; Bories, P. N.; Cynober, L.; Gil, S.; Ferey, G.; Couvreur, P.; Gref, R. *Nat. Mater.* **2010**, *9*, 172.

(7) Horcajada, P.; Gref, R.; Baati, T.; Allan, P. K.; Maurin, G.; Couvreur, P.; Ferey, G.; Morris, R. E.; Serre, C. *Chem. Rev.* **2012**, *112*, 1232.
(8) Coelho, A. *Topas Academic*, Coelho Software, Brisbane, Australia, 2017.
(9) Horcajada, P.; Serre, C.; Vallet-Regi, M.; Sebban, M.; Taulelle, F.; Ferey, G. *Angew. Chem. Int. Ed.* **2006**, *45*, 5974.
(10) Foucault-Collet, A.; Gogick, K. A.; White, K. A.; Villette, S.; Pallier, A.; Collet, G.; Kieda, C.; Li, T.; Geib, S. J.; Rosi, N. L.; Petoud, S. *Proc. Natl. Acad. Sci. USA* **2013**, *110*, 17199.
(11) McKinlay, A. C.; Morris, R. E.; Horcajada, P.; Ferey, G.; Gref, R.; Couvreur, P.; Serre, C. *Angew. Chem. Int. Ed.* **2010**, *49*, 6260.
(12) Lu, K.; He, C.; Lin, W. *J. Am. Chem. Soc.* **2014**, *136*, 16712.
(13) Carne, A.; Carbonell, C.; Imaz, I.; Maspoch, D. *Chem. Soc. Rev.* **2011**, *40*, 291.
(14) Horcajada, P.; Serre, C.; Maurin, G.; Ramsahye, N. A.; Balas, F.; Vallet-Regí, M.; Sebban, M.; Taulelle, F.; Férey, G. *J. Am. Chem. Soc.* **2008**, *130*, 6774.
(15) Cunha, D.; Ben Yahia, M.; Hall, S.; Miller, S. R.; Chevreau, H.; Elkaim, E.; Maurin, G.; Horcajada, P.; Serre, C. *Chem. Mater.* **2013**, *25*, 2767.
(16) Coudert, F.-X. **2015**, *27*, 1905.
(17) Park, J.; Yuan, D.; Pham, K. T.; Li, J.-R.; Yakovenko, A.; Zhou, H.-C. **2012**, *134*, 99.
(18) Lyndon, R.; Konstas, K.; Ladewig Bradley, P.; Southon Peter, D.; Kepert Prof Cameron, J.; Hill Matthew, R. **2013**, *52*, 3695.
(19) Della Rocca, J.; Liu, D. M.; Lin, W. B. *Acc. Chem. Res.* **2011**, *44*, 957.
(20) Bachelder, E. M.; Beaudette, T. T.; Broaders, K. E.; Dashe, J.; Fréchet, J. M. J. *J. Am. Chem. Soc.* **2008**, *130*, 10494.
(21) Broaders, K. E.; Grandhe, S.; Fréchet, J. M. J. *J. Am. Chem. Soc.* **2011**, *133*, 756.
(22) Colson, Y. L.; Grinstaff, M. W. *Adv. Mater.* **2012**, *24*, 3878.
(23) Nguyen, M. M.; Carlini, A. S.; Chien, M. P.; Sonnenberg, S.; Luo, C. L.; Braden, R. L.; Osborn, K. G.; Li, Y. W.; Gianneschi, N. C.; Christman, K. L. *Adv. Mater.* **2015**, *27*, 5547.
(24) Callmann, C. E.; Barback, C. V.; Thompson, M. P.; Hall, D. J.; Mattrey, R. F.; Gianneschi, N. C. *Adv. Mater.* **2015**, *27*, 4611.
(25) Shum, P.; Kim, J. M.; Thompson, D. H. *Adv. Drug Deliv. Rev.* **2001**, *53*, 273.
(26) Yavlovich, A.; Smith, B.; Gupta, K.; Blumenthal, R.; Puri, A. *Mol. Membr. Biol.* **2010**, *27*, 364.
(27) Lux, C. D.; Lux, J.; Collet, G.; He, S.; Chan, M. N.; Olejniczak, J.; Foucault-Collett, A.; Almutairi, A. *Biomacromolecules* **2015**, *16*, 3286.
(28) Purcell, B. P.; Lobb, D.; Charati, M. B.; Dorsey, S. M.; Wade, R. J.; Zellars, K. N.; Doviak, H.; Pettaway, S.; Logdon, C. B.; Shuman, J. A.; Freels, P. D.; Gorman, J. H.; Gorman, R. C.; Spinale, F. G.; Burdick, J. A. *Nat. Mater.* **2014**, *13*, 653.
(29) Kharkar, P. M.; Kiick, K. L.; Kloxin, A. M. *Polym. Chem.* **2015**, *6*, 5565.
(30) Mura, S.; Nicolas, J.; Couvreur, P. *Nat. Mater.* **2013**, *12*, 991.
(31) Viger, M. L.; Collet, G.; Lux, J.; Huu, V. A. N.; Guma, M.; Foucault-Collet, A.; Olejniczak, J.; Joshi-Barr, S.; Firestein, G. S.; Almutairi, A. *Biomaterials* **2017**, *133*, 119.
(32) Viger, M. L.; Sankaranarayanan, J.; de Gracia Lux, C.; Chan, M.; Almutairi, A. *J. Am. Chem. Soc.* **2013**, *135*, 7847.
(33) Ganta, S.; Devalapally, H.; Shahiwala, A.; Amiji, M. *J. Control. Release* **2008**, *126*, 187.
(34) Longmire, M.; Choyke, P. L.; Kobayashi, H. *Nanomedicine* **2008**, *3*, 703.
(35) Balasubramanian, S. K.; Jittiwat, J.; Manikandan, J.; Ong, C. N.; Yu, L. E.; Ong, W. Y. *Biomaterials* **2010**, *31*, 2034.
(36) Epley, C. C.; Roth, K. L.; Lin, S. Y.; Ahrenholtz, S. R.; Grove, T. Z.; Morris, A. J. *Dalton Trans.* **2017**, *46*, 4917.
(37) di Nunzio, M. R.; Agostoni, V.; Cohen, B.; Gref, R.; Douhal, A. *J. Med. Chem.* **2014**, *57*, 411.
(38) Marziyeh, N.; Marta, R.-M.; Gerard, T.; Pérez, B. J.; Ravichandar, B.; Fatemeh, N.; Kristina, K.; W., M. B.; F., C. S.; J., H. A.; C., D. M.; R., H. M. **2016**, *26*, 3244.
(39) Xu, X.-Y.; Chu, C.; Fu, H.; Du, X.-D.; Wang, P.; Zheng, W.; Wang, C.-C. **2018**, *350*, 436.
(40) Huang, N.; Ding, X. S.; Kim, J.; Ihee, H.; Jiang, D. L. *Angew. Chem. Int. Ed.* **2015**, *54*, 8704.
(41) Ito, Y.; Fujita, H. *J. Org. Chem.* **1996**, *61*, 5677.
(42) Nofen, E. M.; Wickham, J.; Koo, B.; Chattopadhyay, A.; Dai, L. L. *Mat. Res. Express* **2016**, *3*.
(43) More, R.; Busse, G.; Hallmann, J.; Paulmann, C.; Scholz, M.; Techert, S. *J. Phys. Chem. C* **2010**, *114*, 4142.
(44) Bouas-Laurent, H.; Castellan, A.; Desvergne, J. P.; Lapouyade, R. *Chem. Soc. Rev.* **2000**, *29*, 43.
(45) Bouas-Laurent, H.; Castellan, A.; Desvergne, J. P.; Lapouyade, R. *Chem. Soc. Rev.* **2001**, *30*, 248.
(46) Casanova, D.; Llunell, M.; Alemany, P.; Alvarez, S. *Chem. Eur. J.* **2005**, *11*, 1479.
(47) Sienkiewicz-Gromiuk, J.; Rusinek, I.; Kurach, Ł.; Rzączyńska, Z. *J. Therm. Anal. Calorim.* **2016**, *126*, 327.
(48) Friedrichs, O. D.; O'Keeffe, M.; Yaghi, O. M. *Acta Cryst. A* **2003**, *59*, 22.
(49) Spek, A. L. *Acta Cryst. D Biol. Cryst.* **2009**, *65*, 148.
(50) Hu, Z. G.; Zhao, D. *Dalton Trans.* **2015**, *44*, 19018.
(51) Zahn, G.; Zerner, P.; Lippke, J.; Kempf, F. L.; Lilienthal, S.; Schroder, C. A.; Schneider, A. M.; Behrens, P. *CrystEngComm* **2014**, *16*, 9198.
(52) Sheldrick, G. M. *Acta Cryst. C Struct. Chem.* **2015**, *71*, 3.
(53) Dolomanov, O. V.; Bourhis, L. J.; Gildea, R. J.; Howard, J. A. K.; Puschmann, H. *J. Appl. Cryst.* **2009**, *42*, 339.
(54) Vandersluis, P.; Spek, A. L. *Acta Cryst. A* **1990**, *46*, 194.

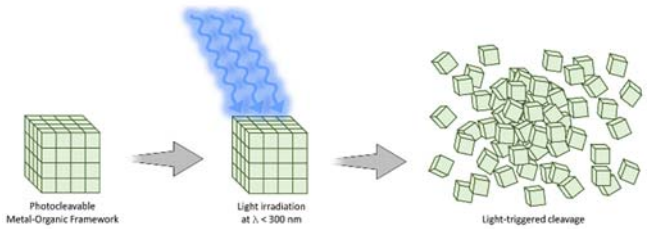
Photocleavable
Metal-Organic Framework
Light irradiation
at λ < 300 nm
Light-triggered cleavage